

Interaction induced reentrance of Bose glass and quench dynamics of Bose gases in twisted bilayer and quasicrystal optical lattices

Shi-Hao Ding^{1,2,3,*}, Li-Jun Lang^{1,2,3,*}, Qizhong Zhu^{2,3,†} and Liang He^{1,2,3,‡}

¹*Institute for Theoretical Physics, School of Physics,*

South China Normal University, Guangzhou 510006, China

²*Key Laboratory of Atomic and Subatomic Structure and Quantum Control (Ministry of Education), Guangdong Basic Research Center of Excellence for Structure and Fundamental Interactions of Matter, School of Physics, South China Normal University, Guangzhou 510006, China and*

³*Guangdong Provincial Key Laboratory of Quantum Engineering and Quantum Materials, Guangdong-Hong Kong Joint Laboratory of Quantum Matter, South China Normal University, Guangzhou 510006, China*

We investigate the ground state and dynamical properties of ultracold gases in optical lattices with an aperiodic external potential—a scenario motivated by recent experiments on twisted bilayer optical lattices and optical quasicrystals. Our study reveals that the interplay between on-site repulsive interactions and a quasiperiodic potential gives rise to rich physics. At low filling factors, increasing the interaction strength induces a delocalization effect that transforms a Bose glass (BG) phase, characterized by disconnected superfluid (SF) regions, into a robust SF phase with a percolated network of SF clusters. This transition is quantitatively characterized by monitoring the percolation probability. At higher filling factors, we uncover a striking reentrant behavior: as the on-site interaction increases, the system initially transitions from BG to SF, but a further increase reverses this trend, returning the system to the BG phase. This reentrance is ascribed to an interaction-driven rearrangement of particles, where a once percolated SF network fragments into isolated SF islands as repulsive interactions dominate. Furthermore, our analysis of quench dynamics demonstrates distinct transient behaviors. Intra-phase quenches yield minimal variations in both the percolation probability and the inverse participation ratio (IPR) of the particle density distribution. In contrast, inter-phase quenches produce pronounced effects; for instance, a quench from the SF to BG phase is marked by an abrupt loss of global SF connectivity, while a BG-to-SF quench features oscillatory changes in the percolation probability and a gradual decrease in the IPR, eventually stabilizing the SF phase. Our findings unveil the complex interplay between disorder and interaction in ultracold Bose gases, offering valuable insights that are highly pertinent to current experimental efforts employing state-of-the-art twisted bilayer and quasicrystalline optical lattice platforms.

I. INTRODUCTION

Recent years, twisted bilayer materials opens a brand new era of twistrionics, which has become a fertile soil for studying and engineering strongly correlation phenomena [1–11]. Most researches focus on the moiré patterns, the commensurate patterns of multiple twisted crystal layers, where the whole system remains certain translational symmetry but the unit cell is much larger than the original one, leading to the flattening of bands and thus, enhancing the interaction effects. Experimentalists have observed in laboratory many emergent strongly correlation effects, such as correlated insulators [1, 2], superconductivity [3], magnetism [4–6], generalized Wigner crystals [7, 8], integer and fractional quantum anomalous Hall insulators [9–16], etc.

On the other hand, the quasicrystal patterns can emerge when the crystal layers are twisted in an incommensurate way that completely breaks the translational symmetry but preserves the long-range order

[17], thereby mediating between the order and disorder. The quasicrystals have been experimentally realized and highly tuned by twisting three layers of graphenes [18] or bilayers of tungsten diselenides [19], but has been less focused before [20, 21] than the commensurate case. It is well known that a quasicrystal would lead to the Anderson localization [22], a phenomenon that lacks the diffusiveness of non-interacting particles when subjected to a random or quasiperiodic potential landscape. In one-dimensional (1D) and two-dimensional (2D) cases, all single-particle eigenstates can be localized by a finite strength of quasicrystal potential [23–25], different from the random disorder where the localization occurs for any infinitesimal strength [26]. Therefore, quasicrystals are ideal platforms for studying localization physics.

Now that the moiré pattern can induce many exotic strongly correlated phenomena, one may wonder how the localization feature in twisted bilayer quasicrystals competes with the interaction. In fermionic systems, most researches focus on the thermal properties of many body localization, especially in 1D case [27–31]. And the incommensurability is also found to radically change the ground state of interacting fermions, compared with the commensurate case [32–37]. In bosonic systems, the interplay of the randomness/quasiperiodicity and the inter-

* These two authors contributed equally to this work.

† qzzhu@m.scnu.edu.cn

‡ liang.he@scnu.edu.cn

action would lead to an exotic many-body ground state—Bose glass (BG) [38, 39], which is insulating like an Anderson insulator, but compressible like a superfluid. Disordered interacting bosons in different dimensions have been studied in various experimental platforms, such as helium films on porous substrates [40], disordered superconducting films [41], doped quantum magnets [42], and especially in optical lattices [43–48]. There are also plenty of theoretical studies for interacting bosons in disordered or quasiperiodic potentials [49–57], and even bosons in interaction-induced disordered or quasiperiodic potentials [58]. However, it is still lacking for the study of interacting bosons in quasicrystals of twisted bilayer optical lattices. Recently, Yu *et al.* experimentally created a 2D octagonal quasicrystalline lattice using four light beams in a plane and one beam in the perpendicular direction, realizing a BG with ultracold atoms in the weakly interacting regime [59, 60].

In this work, we study the ground state and dynamical properties of a class of ultracold bosonic systems realized in optical lattices with an aperiodic external potential—a setting directly inspired by recent experiments on twisted bilayer optical lattices [61] and optical quasicrystals [59]. We investigate how the interplay between on-site repulsive interactions and a quasiperiodic potential drives the system between a homogeneous superfluid (SF) phase and a BG phase. At low filling factors, our findings reveal that an increase in the on-site interaction strength induces a delocalization effect, transforming a BG phase—with disconnected SF regions lacking global connectivity—into a robust SF phase characterized by a percolated network of SF clusters. This phase transition is quantitatively characterized by monitoring the percolation probability (see Fig. 1). At higher filling factors, our results uncover a striking reentrant behavior (see Fig. 2): the system initially undergoes a transition from a BG to an SF phase as the on-site interaction strength increases, but a further increase in the interaction leads to a reversal back to the BG phase. This reentrance is attributed to the interaction-driven rearrangement of particles, wherein a once percolated SF network eventually fragments into isolated SF islands as repulsive interactions become dominant. Moreover, our examination of the system’s quench dynamics reveals distinct transient behaviors (see Fig. 3): while intra-phase quenches produce minimal changes in both the percolation probability and inverse participation ratio (IPR) of the particle density distribution, inter-phase quenches lead to pronounced dynamical effects. Specifically, a quench from the SF to BG phase results in an abrupt loss of global SF connectivity, whereas a BG-to-SF quench is marked by oscillatory changes in the percolation probability and a gradual decrease in the IPR, ultimately stabilizing the SF phase. These findings unveil the rich physics of ultracold Bose gases in optical lattices with an aperiodic external potential, offering valuable insights that are highly relevant for state-of-the-art experiments employing twisted bilayer or quasicrystalline optical lat-

tice platforms.

II. SYSTEM AND MODEL

Inspired by the recent experimental progresses in realizing twisted bilayer optical lattice [61] and optical quasicrystal [59] for ultracold atoms, we consider a single component ultracold bosonic system, the Hamiltonian of which takes the form of a “single-layer” Bose-Hubbard model with an additional external on-site potential, i.e.,

$$\hat{H} = -J \sum_{\langle i,j \rangle} \hat{b}_i^\dagger \hat{b}_j + \frac{U}{2} \sum_i \hat{n}_i (\hat{n}_i - 1) + \sum_i M_i \hat{n}_i, \quad (1)$$

where $\hat{n}_i = \hat{b}_i^\dagger \hat{b}_i$ is the occupation number operator at site i with \hat{b}_i^\dagger (\hat{b}_i) being the corresponding bosonic creation (annihilation) operator, U is the strength of the on-site interaction, and J is the hopping amplitude between nearest-neighbor lattice sites (denoted by $\langle \dots \rangle$). Here, we focus on the case where the underlying optical lattice is a square lattice as it is most relevant for the current experimental set-ups [59, 61]. The last term of \hat{H} is the additional on-site external potential with M_i being its strength at site i . In the experimental set-up that realizes the twisted bilayer optical lattice [61], the on-site external potential M_i takes into account the influences of the lattice on the other layer in the large detuning limit, where the bilayer system can be effectively described by the single-layer model [61, 62]. While in the experimental set-up that realizes the optical quasicrystal [59], M_i simply corresponds to the additional optical lattice potential felt by the atoms. In these regards, the physics of the model Hamiltonian (1) to be discussed in the following is relevant for ultracold twisted bilayer optical lattice systems [61] and optical quasicrystal systems [59] in experiments.

In the following, we focus on the case where M_i assumes the form

$$M_i = M_r \left[\sin^2 (i_x \pi \cos \theta + i_y \pi \sin \theta) + \sin^2 (i_y \pi \cos \theta - i_x \pi \sin \theta) \right], \quad (2)$$

where M_r is the strength of the external potential, i_x (i_y) is the index of the i th site of the square lattice along the x (y) direction, and we choose $\theta = 45^\circ$. This corresponds to the case in the bilayer systems with the twist-angle being 45° [61], or the one in the optical quasicrystal system with the optical lattice formed by superimposing four independent one-dimensional lattices in the x - y plane at 45° angle [59].

The first two terms of the Hamiltonian (1) assume the form of the conventional Bose-Hubbard model [39], they favor two homogeneous phases, namely, the homogeneous SF phase (for large J/U) and Mott insulator phase (for small J/U at integer filling factors) that respect the discrete translation symmetry of the underlying lattice. The

third term of \hat{H} is an aperiodic or a quasiperiodic external potential that explicitly breaks the lattice translation symmetry. Recent investigations [57] showed that this type of terms can give rise to the BG phase that usually arises in disordered bosonic systems [39], due to their aperiodicity. In fact, the interplay between on-site interaction and the quasiperiodic external potential can give rise to much richer physics associated to the BG phase. Particularly, at fixed particle densities which is highly relevant for corresponding experiments, this interplay can give rise to interaction induced reentrant transitions for BG phases and rich quench dynamics as we shall show in the following.

III. RESULTS

To study the ground state of the system described by Hamiltonian (1), we used the bosonic Gutzwiller variational method [63–65]. The variational ground state is assumed to take the site-factorized form $|\text{GW}\rangle = |\phi_1\rangle \otimes \cdots \otimes |\phi_i\rangle \otimes \cdots \otimes |\phi_{N_{\text{lat}}}\rangle$, where each $|\phi_i\rangle$ represents the state at the i -th lattice site, and N_{lat} denotes the total number of sites in the lattice. The individual single-site states $|\phi_i\rangle$ are expanded as a superposition of particle-number eigenstates as $|\phi_i\rangle = \sum_{n=0}^{n_{\text{max}}} C_{i,n} |n\rangle_i$, where n_{max} is the maximum number of particles per site and $C_{i,n}$ are variational parameters that are to be determined by minimizing the total energy of the system. In this work, we focus on the ground state properties of the system at different filling factors $\rho \equiv N/N_{\text{lat}}$, with N being the total number of particles in the system. We examine the system at different filling factors to explore how particle density influences the ground state properties. For the numerical calculations, we set square lattice size $L = 51$, the local maximum truncation number $n_{\text{max}} = 10$, and we employ open boundary conditions for the numerical results if not specified in the text.

A. Transitions between superfluids and Bose glasses

At relatively low filling factors, the typical properties of the system are summarized in Fig. 1, which shows the phase diagram of the system at $\rho \approx 0.04$, along with the particle density distribution $\langle \hat{n}_i \rangle$, the SF order parameter distribution $\langle \hat{b}_i \rangle$, and the discrete field distribution S_i . The latter is used to distinguish between SF and BG phases and will be discussed in detail later. As shown in the lower-left inset of Fig. 1(a), in the low aperiodic potential regime, as expected from the homogeneous Bose-Hubbard model, the system is in the SF phase, with a nonzero SF order parameter $\langle \hat{b}_i \rangle$ that is distributed relatively evenly across the entire lattice. In contrast, in the high aperiodic potential regime, as shown in the upper inset of Fig. 1(a), the system maintains a non-zero SF order parameter $\langle \hat{b}_i \rangle$, but its distribution exhibits a qual-

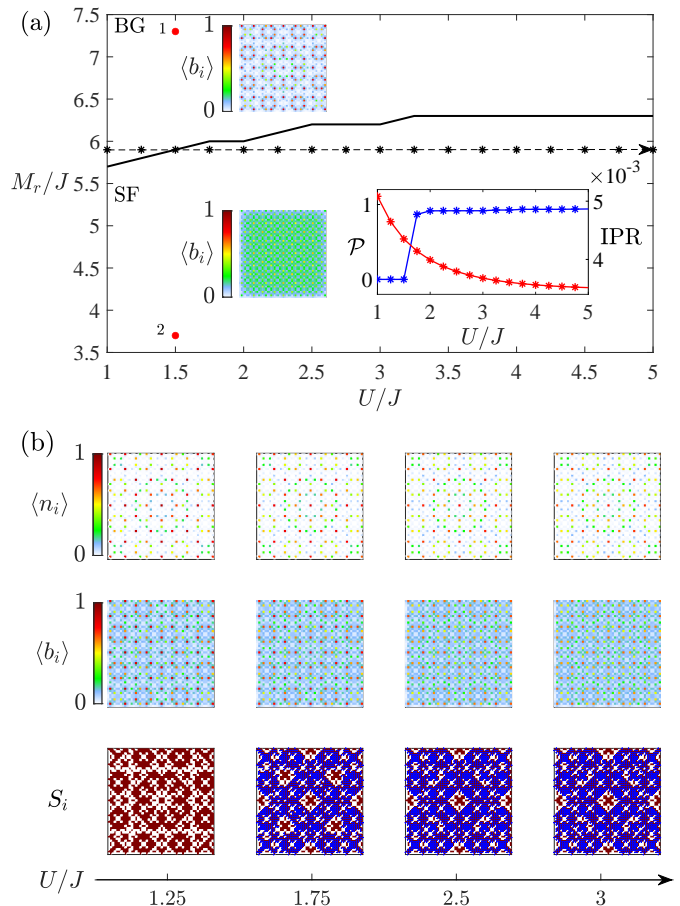


Figure 1. Phase diagram and representative real-space distributions. (a) Phase diagram for a system of 100 particles on a 51×51 square lattice, where the black solid line is the phase boundary between BG (upper) and SF (lower) phases. Inset: Dependence of the percolation probability \mathcal{P} (blue curve) and the inverse participation ratio (IPR) (red curve) on U/J for points along the dotted line indicated in the phase diagram. The inserted SF order parameter distributions correspond to the nearby red points marked in the figure. (b) Real-space distributions of the particle density $\langle \hat{n}_i \rangle$, SF order parameter $\langle \hat{b}_i \rangle$ and the discrete field S_i near the phase boundary ($M_r/J = 5.9$). See text for more details.

itatively different structure. In particular, although the SF order parameter is nonzero in various regions, these regions are “disconnected” from each other, indicating a transition to a new phase: the BG phase, which is absent in conventional homogeneous systems of lattice bosons.

To quantitatively distinguish the SF phase from the BG phase, we employ the percolation method [57, 66–69], a widely used technique for studying phase transitions in disordered or quasi-disordered systems. The key quantity used to differentiate the SF and BG phases is the percolation probability \mathcal{P} , with $\mathcal{P} = 0$ indicating no connected SF region spanning the entire system (signifying the BG phase), and $\mathcal{P} > 0$ indicating the presence of a percolated SF region (signifying the SF phase spanning

the entire system). In this work, we adopt the method from [57, 69], where \mathcal{P} is calculated using the corresponding discrete field S_i [69], which is constructed from both the particle density distribution $\langle \hat{n}_i \rangle$ and the SF order parameter distribution $\langle \hat{b}_i \rangle$. This field encapsulates the percolation properties of the SF regions in the system (see Appendix A for technical details on extracting \mathcal{P} from S_i). For example, in the last row of Fig. 1(b), red-marked sites represent various connected SF regions that do not span the entire system, while blue-marked sites correspond to connected SF regions that do span the entire system, forming a percolated SF region.

From Fig. 1(a), we observe that tuning the on-site interaction strength U can drive the transition between the SF and BG phases in the high aperiodic potential regime. As indicated by the horizontal arrow in Fig. 1(a) and the corresponding distributions for $\langle \hat{n}_i \rangle$, $\langle \hat{b}_i \rangle$, and S_i in Fig. 1(b) at a fixed aperiodic potential strength M_r , the system transitions from the BG phase with $\mathcal{P} = 0$ at relatively small U to the SF phase with a finite percolation probability \mathcal{P} at larger U [see the lower-right inset of Fig. 1(a)]. This transition is driven by the “delocalization” effect of the repulsive on-site interaction. As seen in the lower-right inset of Fig. 1(a), the IPR for the normalized density distribution $\langle \hat{n}_i \rangle \equiv \langle \hat{n}_i \rangle / \sum_{i=1}^{N_{\text{lat}}} \langle \hat{n}_i \rangle$ directly characterizes the extent of localization in the system, i.e., $\text{IPR} \equiv \sum_{i=1}^{N_{\text{lat}}} \langle \hat{n}_i \rangle^2$. The IPR decreases as U increases, reflecting the delocalization of the particles. At relatively small U , the SF regions are localized [see the left most plot for S_i in Fig. 1(b)]. As U increases, the SF regions expand, and at large enough U , they can merge, forming a percolated SF region that drives the system into the SF phase.

B. Reentrance between superfluid and Bose glass phases

In the previous section, we discussed the system at relatively low filling factors. From the particle density distribution in Fig. 1(b), we observe that the average number of particles per lattice site is less than 1, indicating the influence of the on-site interaction is very weak. This thus raises the question of whether different physical phenomena might arise when the system’s filling factor is higher. To explore this, we present the results for a system with a filling factor $\rho = 0.08$, and the corresponding results are summarized in Fig. 2, which includes the phase diagram and typical real-space distributions. Compared to the phase diagram at low filling factors, we observe a reentrant transition at higher filling factors, as shown in Fig. 2(a). Focusing on the dotted line in this phase diagram, we see that as the on-site interaction U increases, the system first transitions from the BG phase to the SF phase. However, as U continues to increase, the system transitions back from the SF phase to the BG phase. This indicates that the on-site

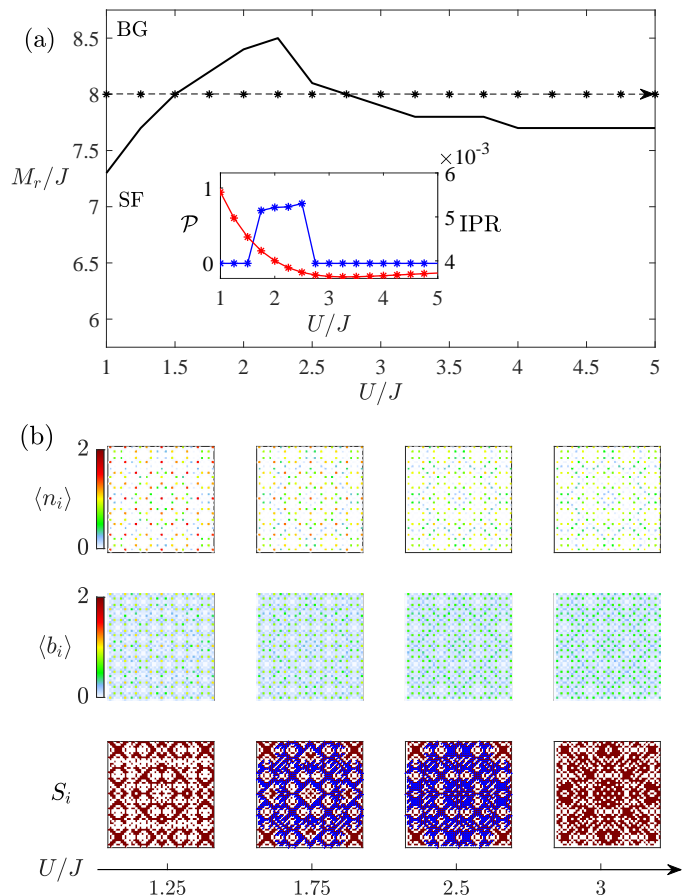


Figure 2. Phase diagram and representative real-space distributions. (a) Phase diagram for a system of 196 particles on a 51×51 square lattice, where the black solid line is the phase boundary between BG (upper) and SF (lower) phases. Inset: Dependence of the percolation probability \mathcal{P} (blue curve) and IPR (red curve) on U/J for points along the dotted line indicated in the phase diagram. (b) Real-space distributions of the particle density $\langle n_i \rangle$, SF order parameter $\langle b_i \rangle$ and the discrete field S_i near the phase boundary ($M_r/J = 8$). See text for more details.

interaction can drive a reentrant transition to the BG phase.

To understand this reentrant behavior, let us first check the typical real-space distributions of the system as U changes are shown in Fig. 2(b). When the on-site interaction $U/J = 1.25$ is relatively small compared to the external potential field strength $M_r/J = 8$, the system consists of isolated SF clusters. As we gradually increase the on-site interaction to $U/J = 1.75$, a percolated SF region (marked in blue) appears in the S_i distribution shown in Fig. 2(b), indicating that the system has transitioned from the BG phase to the SF phase.

The mechanism of this stage of transition is actually similar to the one of the lower filling case presented in Sec.III A. Specifically, when the on-site interaction U increases, the most significant interaction effect occurs at

lattice sites where the average number of particles is greater than 1. At these sites, the particles repel each other, leading to a redistribution. As a result, SF paths emerge during this repulsion process, and the system transitions from the BG phase to the SF phase.

However, as we further increase $U/J = 3$, the system exhibits behavior different from that at low filling factors. As shown in the lower right plot of Fig. 2(b), the percolated SF region disappears from the distribution of S_i at $U/J = 3$, indicating the system transitions from the SF phase back to the BG phase again. To understand this stage of transition, we notice that although percolated SF regions can form in the SF phase, the increasing repulsive interaction strength can still cause the particle density distribution to undergo further rearrangement, causing percolated SF regions breaking up into isolated SF islands, thus driving the system entering the BG phase again. However, if particle density of each site is sufficiently low, this would indicate the local state of each site only consists of zero or single occupation state. As a consequence, further increasing on-site interaction strength can hardly impose any physical influence on the system, which is consistent with what we can observe in the last three columns of plot shown in Fig. 1(b) for the low filling case. In fact, at even high filling factors, one can observe even more times of the reentrance (see Appendix B for more numerical results at even higher filling factors).

C. Quench dynamics

Thus far, we have focused on the static properties of the system. Now let us turn to the dynamical properties, in particular, here we shall focus on the quench dynamics of the system. Specifically, via time-dependent Gutzwiller approach [70–72] (see Appendix C for technique details of the approach), we investigate the quench dynamics of two different types, namely, intra-phase quench and inter-phase quench.

For intra-phase quenches, where the system remains within the same phase (e.g., from the BG/SF phase to the BG/SF phase), we observe no qualitative changes in the system’s dynamics. As shown in Fig. 3, neither the time evolution of IPR nor the percolation probability \mathcal{P} exhibit significant changes [see Figs. 3(b, c)]. Similarly, the typical SF order parameter and the discrete field distributions at different time instants remain largely unchanged [see Fig. 3(d)].

For inter-phase quenches, where the system undergoes a transition between different phases (e.g., from SF to BG, or vice versa), we observe more significant qualitative changes. Specifically, for these quenches, the initial state corresponds to the ground state configuration at the two red dots in Fig. 3(a) with $(U/J = 2, M_r/J = 5)$ in the SF phase and $(U/J = 2, M_r/J = 10)$ in the BG phase. In the quench from the SF phase to the BG phase, the percolation probability \mathcal{P} [illustrated by the green line in Fig. 3(c)] rapidly decreases from nearly 1 to 0,

indicating the swift transition of the system from SF to BG. Once the system reaches the BG phase, \mathcal{P} remains at 0, reflecting that the system remains in the BG phase. This behavior arises because the BG phase consists of isolated SF islands, which restrict particle movement to these disconnected regions. As a result, the IPR remains relatively constant with only minor fluctuations, corresponding to slight variations in the spatial distribution of particles over time [see the green line in Fig. 3(b)].

For the quench from the BG phase to the SF phase, the percolation probability \mathcal{P} fluctuates between 0 and non-zero values for times $tJ > 5$, signaling the system’s transition between the BG and SF phases [see the blue line in Fig. 3(c)]. Unlike the quench from SF to BG, where particles are confined to isolated SF islands, in the BG-to-SF quench, particles can move freely between SF clusters, allowing the formation of SF paths. However, at certain moments, the system may lose its SF path and transition back to the BG phase. This phenomenon gradually fades over time, and as shown in Fig. 3, the periods during which $\mathcal{P} = 0$ become shorter, eventually leading the system to settle into a steady SF phase. This trend is also reflected in the time evolution of the IPR in Fig. 3(b). Initially, in the BG phase, the particles are localized at specific lattice sites, resulting in a relatively large IPR. As the system evolves, particles diffuse through space, causing a gradual decrease in the IPR. Although the IPR may occasionally increase, it generally decreases over time, indicating that the system is eventually transitioning to the SF phase.

IV. CONCLUSIONS

Our work demonstrates that ultracold bosonic systems in optical lattices with an aperiodic external potential exhibit a rich interplay between disorder and interaction effects. We have shown that at low filling factors, an increase in the on-site repulsive interaction triggers a delocalization process that transforms a BG phase, characterized by isolated and disconnected SF regions, into a robust SF phase with a percolated network. This transition is clearly evidenced by the evolution of the percolation probability and IPR. At higher filling factors, we uncover a striking reentrant behavior wherein the system initially transitions from a BG to a SF phase as the interaction strength increases, but further enhancement of the interaction causes the SF network to fragment, reverting the system back to a BG phase. Moreover, our analysis of quench dynamics reveals markedly different transient behaviors for intra-phase and inter-phase quenches, highlighting the sensitive dependence of the system’s dynamical evolution on the initial state and interaction parameters. These findings not only deepen our understanding of localization phenomena in interacting Bose gases but also offer valuable insights for ongoing experiments utilizing twisted bilayer and quasicrystalline optical lattice platforms, where tuning disorder and interaction effects

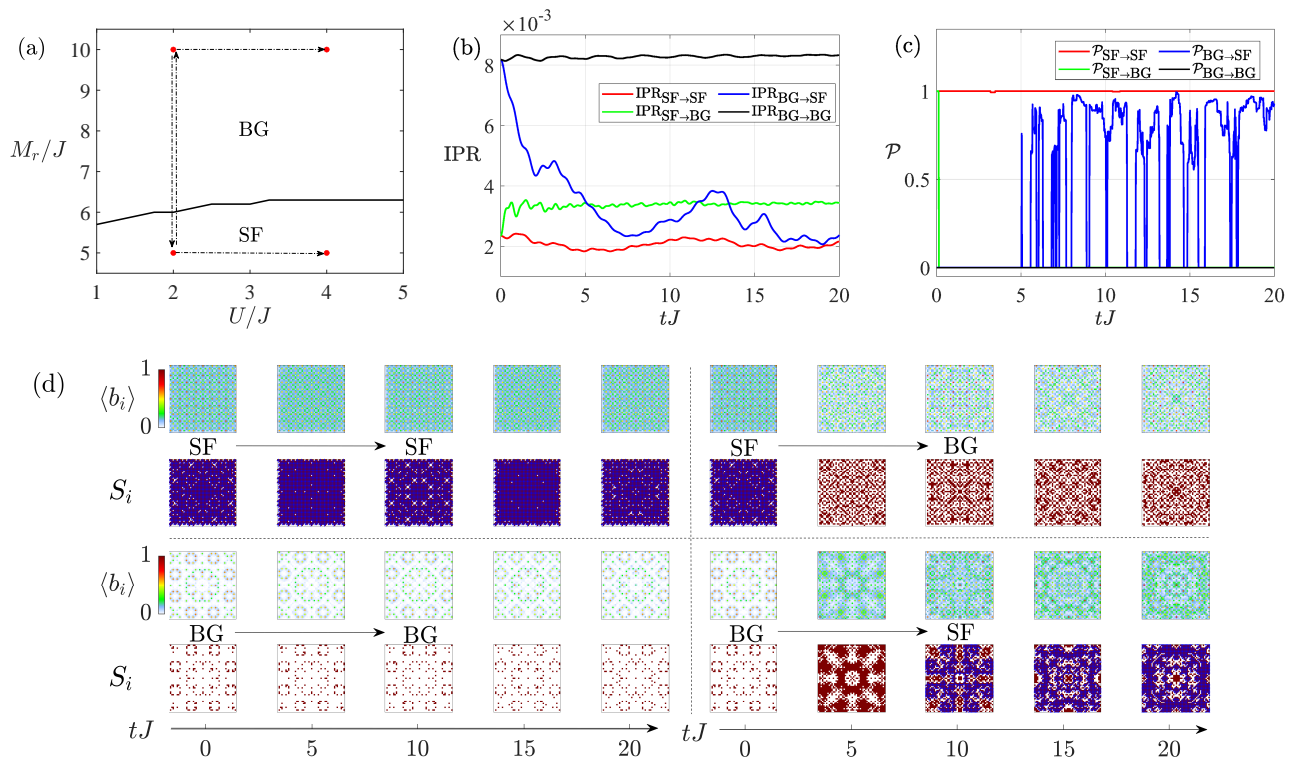


Figure 3. (a) Phase diagram of the system at $N = 100$ with quench directions marked with arrows. (b) Time dependence of IPR of the corresponding quench dynamics. (c) Time dependence of percolation probability \mathcal{P} of the corresponding quench dynamics. (d) Typical SF order parameter and discrete field distributions during different quench processes marked in (a). See text for more details.

is pivotal for exploring novel many-body phases.

ACKNOWLEDGMENTS

This work is supported by the NKRDPC (Grant No. 2022YFA1405304), NSFC (Grant Nos. 12275089 and 12004118), and the Guangdong Basic and Applied Basic Research Foundation (Grants Nos. 2024A1515010188, 2023A1515012800, and 2021A1515010212), and Guangdong Provincial Key Laboratory (Grant No. 2020B1212060066).

Appendix A: TECHNICAL DETAILS ON CALCULATING PERCOLATION PROBABILITY FROM DISCRETE FILED

In this appendix, we provide technique details on calculating the percolation probability \mathcal{P} from the discrete field S_i . The percolation probability \mathcal{P} is defined in Reference [57] as

$$\mathcal{P} = \frac{N_{\text{span}}}{N_{\varphi}}, \quad (\text{A1})$$

where N_{span} is the number of SF sites in a percolating cluster, and N_{φ} is the total number of sites with finite

φ . In our numerical calculations, N_{span} and N_{φ} are derived from the discrete field S_i [69], which can be constructed by the particle density distribution $\langle \hat{n}_i \rangle$ and SF order parameter distribution $\langle \hat{b}_i \rangle$ described in the main text. Specifically, we label sites with integer occupancy numbers as MI sites ($S_i = 0$) and sites with non-integer occupancy numbers as SF sites ($S_i = 1$). According to the definition of S_i , N_{φ} corresponds to the total number of sites where $S_i = 1$, i.e., $N_{\varphi} = \sum_i^{N_{\text{lat}}} S_i$. To calculate N_{span} , it is necessary to identify the percolating cluster. The criterion for percolation, as outlined in [73], is the existence of at least one SF path that spans the entire system, either from left to right or from top to bottom. Once such an SF path is identified, the SF cluster that contains this SF path is considered the percolating cluster. The total number of lattice sites in this percolating cluster is then defined as N_{span} . Clearly, as shown by the calculation of the percolation probability \mathcal{P} described above, this quantity can be used to distinguish the SF phase from the BG phase. In the BG phase, there are no percolating SF clusters, which results in a percolation probability of 0. In contrast, in the SF phase, the presence of percolating SF clusters leads to a non-zero percolation probability.

Appendix B: NUMERICAL RESULTS AT EVEN HIGHER FILLING FACTORS

As discussed in the main text, we hypothesized that multiple reentrance phenomena could be observed in the system with an even higher particle filling. Indeed, as anticipated, this behavior is demonstrated in Fig. 4 below.

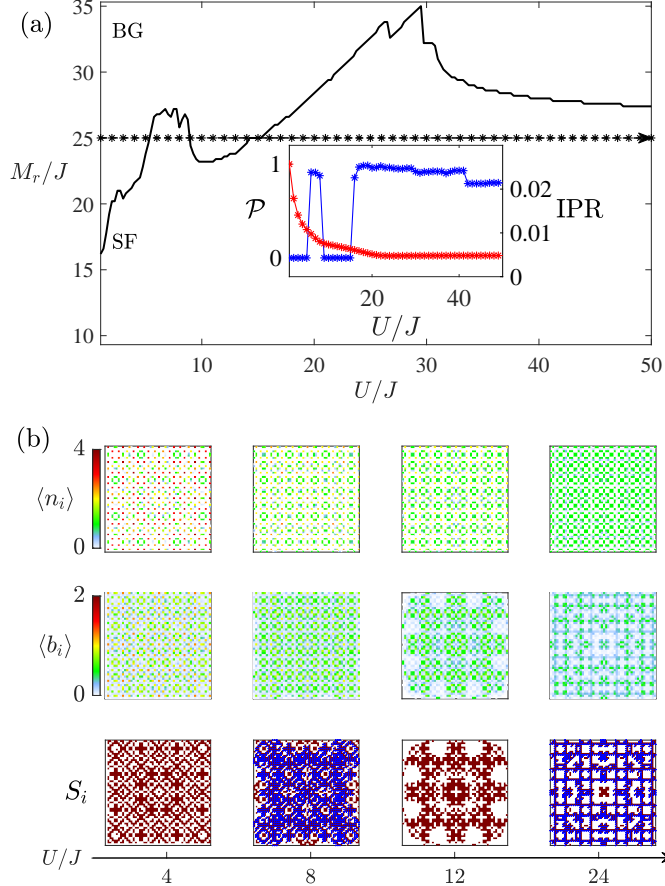


Figure 4. Phase diagram and representative real-space distributions. (a) Phase diagram for a system of 1024 particles on a 51×51 square lattice. Inset: Dependence of the percolation probability \mathcal{P} (blue curve) and IPR (red curve) on U/J for points along the dotted line indicated in the phase diagram. (b) Configurations of the particle density distribution $\langle n_i \rangle$, SF order parameter distribution $\langle b_i \rangle$ and the discrete field S_i of four points on the dotted line ($M_r/J = 25$). See text for more details.

We plotted the phase diagram for a particle filling of 1024, which reveals two distinct peaks. Additionally, we included a series of real-space distribution diagrams showing the effect of varying the interaction strength U on the lattice, with the changes in U indicated by the horizontal lines in the phase diagram. As shown in the inset of the phase diagram, the percolation probability of the ground state exhibits multiple transitions between

0 and non-zero values, corresponding to the system's behavior as it transitions from the BG phase to the SF phase, then back to the BG phase, and finally returning to the SF phase. The particle density distribution diagram Fig. 4(b) further illustrates that, as the particle filling increases, the system undergoes more significant changes due to the enhanced on-site interaction strength. Moreover, these changes lead to the formation and annihilation of SF path, creating a more complex phase transition process.

Appendix C: Time dependent Gutzwiller approach

In this appendix, we present the technique details of the time-dependent Gutzwiller approach [70–72]. This approach is built on top of the static Gutzwiller approach. The static Gutzwiller method is employed to determine the ground state by minimizing the total energy of the system, given by $E(\{C_{i,n}\}) = \langle \text{GW} | \hat{H} | \text{GW} \rangle$, while the dynamic Gutzwiller method minimizes the action to simulate the system's evolution. Specifically, by applying the variational principle, we can write the action of the system as $S = \int dt \left[-i \langle \text{GW}(t) | \partial_t | \text{GW}(t) \rangle + \langle \text{GW}(t) | \hat{H} | \text{GW}(t) \rangle \right]$. Variation with respect to any of the coefficients $C_{i,n}(t)$ yields the equation of motion:

$$i\partial_t C_{i,n}(t) = C_{i,n}(t) \left[\frac{U}{2} n(n-1) + M_i n \right] - J \left[C_{i,n+1} \sqrt{n_l+1} \left(\sum_j \Phi_j^* \right) + C_{i,n-1} \sqrt{n_l} \left(\sum_j \Phi_j \right) \right] \quad (\text{C1})$$

where $\sum_j \Phi_j = \sum_j \sum_{n=0}^{n_{\max}-1} C_{j,n+1} C_{j,n}^* \sqrt{n+1}$ and \sum_j denotes the sum over neighboring lattice points.

Since the time-dependent Gutzwiller method effectively conserves particle number, we can numerically simulate the system's evolution once the equations of motion for the wavefunction coefficients are obtained. By analyzing typical real-space distributions at different times, we can investigate the system's dynamical characteristics. This can be illustrated by considering an arbitrary initial Gutzwiller state $|\text{GW}(0)\rangle$. After a time step dt , the state becomes:

$$|\text{GW}(dt)\rangle = |\text{GW}(0)\rangle - idt\hat{H}|\text{GW}(0)\rangle \quad (\text{C2})$$

The expected value of the particle number at the next

time step is:

$$\begin{aligned}
 \langle \hat{N}(dt) \rangle &= \langle \text{GW}(dt) | \hat{N} | \text{GW}(dt) \rangle \\
 &= \langle \hat{N}(0) \rangle + idt \langle \text{GW}(0) | [\hat{H}, \hat{N}] | \text{GW}(0) \rangle \\
 &\quad + \mathcal{O}(dt^2).
 \end{aligned}
 \tag{C3}$$

The fact that particle number is not exactly conserved, but only on average, is reflected in the commutator of the second term, which does not vanish exactly, but whose expectation value is zero for any arbitrary state.

-
- [1] Y. Cao, V. Fatemi, A. Demir, S. Fang, S. L. Tomarken, J. Y. Luo, J. D. Sanchez-Yamagishi, K. Watanabe, T. Taniguchi, E. Kaxiras, R. C. Ashoori, and P. Jarillo-Herrero, *Nature* **556**, 80 (2018).
- [2] T. Li, S. Jiang, L. Li, Y. Zhang, K. Kang, J. Zhu, K. Watanabe, T. Taniguchi, D. Chowdhury, L. Fu, J. Shan, and K. F. Mak, *Nature* **597**, 350 (2021).
- [3] Y. Cao, V. Fatemi, S. Fang, K. Watanabe, T. Taniguchi, E. Kaxiras, and P. Jarillo-Herrero, *Nature* **556**, 43 (2018).
- [4] C. Gong, L. Li, Z. Li, H. Ji, A. Stern, Y. Xia, T. Cao, W. Bao, C. Wang, Y. Wang, Z. Q. Qiu, R. J. Cava, S. G. Louie, J. Xia, and X. Zhang, *Nature* **546**, 265 (2017).
- [5] B. Huang, G. Clark, E. Navarro-Moratalla, D. R. Klein, R. Cheng, K. L. Seyler, D. Zhong, E. Schmidgall, M. A. McGuire, D. H. Cobden, W. Yao, D. Xiao, P. Jarillo-Herrero, and X. Xu, *Nature* **546**, 270 (2017).
- [6] G. Chen, A. L. Sharpe, E. J. Fox, Y.-H. Zhang, S. Wang, L. Jiang, B. Lyu, H. Li, K. Watanabe, T. Taniguchi, Z. Shi, T. Senthil, D. Goldhaber-Gordon, Y. Zhang, and F. Wang, *Nature* **579**, 56 (2020).
- [7] H. Li, S. Li, E. C. Regan, D. Wang, W. Zhao, S. Kahn, K. Yumigeta, M. Blei, T. Taniguchi, K. Watanabe, S. Tongay, A. Zettl, M. F. Crommie, and F. Wang, *Nature* **597**, 650 (2021).
- [8] E. C. Regan, D. Wang, C. Jin, M. I. Bakti Utama, B. Gao, X. Wei, S. Zhao, W. Zhao, Z. Zhang, K. Yumigeta, M. Blei, J. D. Carlström, K. Watanabe, T. Taniguchi, S. Tongay, M. Crommie, A. Zettl, and F. Wang, *Nature* **579**, 359 (2020).
- [9] M. Serlin, C. L. Tschirhart, H. Polshyn, Y. Zhang, J. Zhu, K. Watanabe, T. Taniguchi, L. Balents, and A. F. Young, *Science* **367**, 900 (2020).
- [10] T. Li, S. Jiang, B. Shen, Y. Zhang, L. Li, Z. Tao, T. Devakul, K. Watanabe, T. Taniguchi, L. Fu, J. Shan, and K. F. Mak, *Nature* **600**, 641 (2021).
- [11] Y. Zhou, J. Sung, E. Brutschea, I. Esterlis, Y. Wang, G. Scuri, R. J. Gelly, H. Heo, T. Taniguchi, K. Watanabe, G. ZarÁnd, M. D. Lukin, P. Kim, E. Demler, and H. Park, *Nature* **595**, 48 (2021).
- [12] J. Cai, E. Anderson, C. Wang, X. Zhang, X. Liu, W. Holtzmann, Y. Zhang, F. Fan, T. Taniguchi, K. Watanabe, Y. Ran, T. Cao, L. Fu, D. Xiao, W. Yao, and X. Xu, *Nature* **622**, 63 (2023).
- [13] H. Park, J. Cai, E. Anderson, Y. Zhang, J. Zhu, X. Liu, C. Wang, W. Holtzmann, C. Hu, Z. Liu, T. Taniguchi, K. Watanabe, J.-H. Chu, T. Cao, L. Fu, W. Yao, C.-Z. Chang, D. Cobden, D. Xiao, and X. Xu, *Nature* **622**, 74 (2023).
- [14] Y. Zeng, Z. Xia, K. Kang, J. Zhu, P. Knüppel, C. Vaswani, K. Watanabe, T. Taniguchi, K. F. Mak, and J. Shan, *Nature* **622**, 69 (2023).
- [15] F. Xu, Z. Sun, T. Jia, C. Liu, C. Xu, C. Li, Y. Gu, K. Watanabe, T. Taniguchi, B. Tong, J. Jia, Z. Shi, S. Jiang, Y. Zhang, X. Liu, and T. Li, *Phys. Rev. X* **13**, 031037 (2023).
- [16] Z. Lu, T. Han, Y. Yao, A. P. Reddy, J. Yang, J. Seo, K. Watanabe, T. Taniguchi, L. Fu, and L. Ju, *Nature* **626**, 759 (2024).
- [17] D. Shechtman, I. Blech, D. Gratias, and J. W. Cahn, *Phys. Rev. Lett.* **53**, 1951 (1984).
- [18] A. Uri, S. C. de la Barrera, M. T. Randeria, D. Rodan-Legrain, T. Devakul, P. J. D. Crowley, N. Paul, K. Watanabe, T. Taniguchi, R. Lifshitz, L. Fu, R. C. Ashoori, and P. Jarillo-Herrero, *Nature (London)* **620**, 762 (2023).
- [19] Y. Li, F. Zhang, V.-A. Ha, Y.-C. Lin, C. Dong, Q. Gao, Z. Liu, X. Liu, S. H. Ryu, H. Kim, C. Jozwiak, A. Bostwick, K. Watanabe, T. Taniguchi, B. Kousa, X. Li, E. Rotenberg, E. Khalaf, J. A. Robinson, F. Giustino, and C.-K. Shih, *Nature (London)* **625**, 494 (2024).
- [20] M. J. Park, H. S. Kim, and S. Lee, *Phys. Rev. B* **99**, 245401 (2019).
- [21] B. Huang and W. V. Liu, *Phys. Rev. B* **100**, 144202 (2019).
- [22] P. W. Anderson, *Phys. Rev.* **109**, 111124-3 (1958).
- [23] S. Aubry and G. André, *Ann. Israel. Phys. Soc.* **3**, 133 (1980).
- [24] G. Roati, C. D’Errico, L. Fallani, M. Fattori, C. Fort, M. Zaccanti, G. Modugno, M. Modugno, and M. Inguscio, *Nature* **453**, 895 (2008).
- [25] Y. Lahini, R. Pugatch, F. Pozzi, M. Sorel, R. Morandotti, N. Davidson, and Y. Silberberg, *Phys. Rev. Lett.* **103**, 013901 (2009).
- [26] E. Abrahams, P. W. Anderson, D. C. Licciardello, and T. V. Ramakrishnan, *Phys. Rev. Lett.* **42**, 140405-1 (1979).
- [27] S. Iyer, V. Oganessian, G. Refael, and D. A. Huse, *Phys. Rev. B* **87**, 134202 (2013).
- [28] R. Mondaini and M. Rigol, *Phys. Rev. A* **92**, 041601 (2015).
- [29] S. Xu, X. Li, Y.-T. Hsu, B. Swingle, and S. Das Sarma,

- Phys. Rev. Res. **1**, 032039 (2019).
- [30] D. Vu, K. Huang, X. Li, and S. Das Sarma, Phys. Rev. Lett. **128**, 146601 (2022).
- [31] Y. Wang, C. Cheng, X.-J. Liu, and D. Yu, Phys. Rev. Lett. **126**, 080602 (2021).
- [32] D. Vu and S. Das Sarma, Phys. Rev. Lett. **126**, 036803 (2021).
- [33] M. Gonçalves, B. Amorim, F. Riche, E. V. Castro, and P. Ribeiro, Nat. Phys. **20**, 1933 (2024).
- [34] Y. E. Kraus, O. Zilberberg, and R. Berkovits, Phys. Rev. B **89**, 161106 (2014).
- [35] T. Cookmeyer, J. Motruk, and J. E. Moore, Phys. Rev. B **101**, 174203 (2020).
- [36] R. Oliveira, M. Gonçalves, P. beiro, E. V. Castro, and B. Amorim, arXiv:2303.17656 (2024).
- [37] M. Gonçalves, J. H. Pixley, B. Amorim, E. V. Castro, and P. Ribeiro, Phys. Rev. B **109**, 014211 (2024).
- [38] T. Giamarchi and H. J. Schulz, Phys. Rev. B **37**, 325 (1988).
- [39] M. P. A. Fisher, P. B. Weichman, G. Grinstein, and D. S. Fisher, Phys. Rev. B **40**, 546 (1989).
- [40] P. A. Crowell, F. W. Van Keuls, and J. D. Reppy, Phys. Rev. B **55**, 12620 (1997).
- [41] B. Sacépé, T. Dubouchet, C. Chapelier, M. Sanquer, M. Ovadia, D. Shahar, M. Feigel'man, and L. Ioffe, Nat. Phys. **7**, 239 (2011).
- [42] R. Yu, L. Yin, N. S. Sullivan, J. S. Xia, C. Huan, A. Paduan-Filho, N. F. Oliveira Jr, S. Haas, A. Steppke, C. F. Miclea, F. Weickert, R. Movshovich, E.-D. Mun, B. L. Scott, V. S. Zapf, and T. Roscilde, Nature (London) **489**, 379 (2012).
- [43] L. Fallani, J. E. Lye, V. Guarrera, C. Fort, and M. Inguscio, Phys. Rev. Lett. **98**, 130404 (2007).
- [44] B. Deissler, M. Zaccanti, G. Roati, C. D'Errico, M. Fattori, M. Modugno, G. Modugno, and M. Inguscio, Nat. Phys. **6**, 354 (2010).
- [45] M. Pasienski, D. McKay, M. White, and B. DeMarco, Nat. Phys. **6**, 677 (2010).
- [46] B. Gadway, D. Pertot, J. Reeves, M. Vogt, and D. Schneble, Phys. Rev. Lett. **107**, 145306 (2011).
- [47] C. D'Errico, E. Lucioni, L. Tanzi, L. Gori, G. Roux, I. P. McCulloch, T. Giamarchi, M. Inguscio, and G. Modugno, Phys. Rev. Lett. **113**, 095301 (2014).
- [48] C. Meldgin, U. Ray, P. Russ, D. Chen, D. M. Ceperley, and B. DeMarco, Nat. Phys. **12**, 646 (2016).
- [49] S. Rapsch, U. Schollwöck, and W. Zwerger, Europhys. Lett. **46**, 559 (1999).
- [50] G. Roux, T. Barthel, I. P. McCulloch, C. Kollath, U. Schollwöck, and T. Giamarchi, Phys. Rev. A **78**, 023628 (2008).
- [51] U. Bissbort and W. Hofstetter, Europhys. Lett. **86**, 50007 (2009).
- [52] Ş. G. Söyler, M. Kiselev, N. V. Prokof'ev, and B. V. Svistunov, Phys. Rev. Lett. **107**, 185301 (2011).
- [53] A. E. Niederle and H. Rieger, Phys. Rev. A **91**, 043632 (2015).
- [54] C. Zhang, A. Safavi-Naini, and B. Capogrosso-Sansone, Phys. Rev. A **91**, 031604 (2015).
- [55] M. Gerster, M. Rizzi, F. Tschirsich, P. Silvi, R. Fazio, and S. Montangero, New J. Phys. **18**, 015015 (2016).
- [56] H. Yao, T. Giamarchi, and L. Sanchez-Palencia, Phys. Rev. Lett. **125**, 060401 (2020).
- [57] D. Johnstone, P. Ohberg, and C. W. Duncan, J. Phys. A **54**, 395001 (2021).
- [58] J.-H. Zeng, Q. Zhu, and L. He, arXiv:2405.24732 (2024).
- [59] J.-C. Yu, S. Bhave, L. Reeve, B. Song, and U. Schneider, Nature (London) **633**, 338 (2024).
- [60] R. Gautier, H. Yao, and L. Sanchez-Palencia, Phys. Rev. Lett. **126**, 110401 (2021).
- [61] Z. Meng, L. Wang, W. Han, F. Liu, K. Wen, C. Gao, P. Wang, C. Chin, and J. Zhang, Nature (London) **615**, 231 (2023).
- [62] X.-T. Wan, C. Gao, and Z.-Y. Shi, arXiv:2404.08211 (2024).
- [63] W. Krauth, M. Caffarel, and J.-P. Bouchaud, Phys. Rev. B **45**, 3137 (1992).
- [64] D. Jaksch, C. Bruder, J. I. Cirac, C. W. Gardiner, and P. Zoller, Phys. Rev. Lett. **81**, 3108 (1998).
- [65] N. Lanatà, H. U. R. Strand, X. Dai, and B. Hellsing, Phys. Rev. B **85**, 035133 (2012).
- [66] K. Sheshadri, H. R. Krishnamurthy, R. Pandit, and T. V. Ramakrishnan, Phys. Rev. Lett. **75**, 4075 (1995).
- [67] P. Buonsante, F. Massel, V. Penna, and A. Vezzani, Phys. Rev. A **79**, 013623 (2009).
- [68] B. M. Kumburi and V. W. Scarola, Phys. Rev. B **85**, 020501 (2012).
- [69] A. Niederle and H. Rieger, New J. Phys. **15**, 075029 (2013).
- [70] M. Schiró and M. Fabrizio, Phys. Rev. Lett. **105**, 076401 (2010).
- [71] I. Bloch, J. Dalibard, and W. Zwerger, Rev. Mod. Phys. **80**, 885 (2008).
- [72] J. Zakrzewski, Phys. Rev. A **71**, 043601 (2005).
- [73] A. Barman, S. Dutta, A. Khan, and S. Basu, Eur. Phys. J. B **86**, 1 (2013).